



Nitrogen and sulfur co-doped carbon cryogel electrode for membrane capacitive deionization

Ling Liu^a, Wendan Cui^a, Qinghan Meng^{a,*}, Guiying Tian^{b,*}

^aThe Key Laboratory of Beijing City on Preparation and Processing of Novel Polymer Materials, Beijing University of Chemical Technology, Beijing 100029, China, Tel. +86 13522090517, email: ll@mail.buct.edu.cn (L. Liu), 752204377@qq.com (W. Cui), qhmeng@mail.buct.edu.cn (Q. Meng)

^bInstitute for Applied Materials, Karlsruhe Institute of Technology, Hermann-von-Helmholtz-Platz 1, 76344 Eggenstein-Leopoldshafen, Germany, Tel. +49 17645983055, email: guiying.tian@partner.kit.edu (G. Tian)

Received 14 January 2018; Accepted 13 September 2018

ABSTRACT

Capacitive deionization with porous carbon has shown a strong ability to remove various inorganic species from aqueous solutions. In this paper, we propose a novel sulfur-nitrogen doped carbon cryogel form membrane capacitive deionization electrodes. The carbon cryogel is prepared via the polycondensation of thiourea, resorcinol and formaldehyde in a weakly alkaline aqueous solution followed by a pyrolysis process at 800°C. The present work focuses on the influence of dual doping on the structure and electrosorption properties. Also, adsorption capacities of the doped carbon cryogel electrode in the capacitive deionization mode and the membrane capacitive deionization mode are compared. The results confirm that the carbon cryogel prepared with thiourea/resorcinol molar ratio of 0.2:1 displays high specific capacitance (182 F/g), maximum adsorption capacity (37.16 mg/g) and higher charge efficiency (65.8%) at 1.8 V in the membrane capacitive deionization. The Freundlich isothermal model is suitable to simulate the adsorption behavior of NaCl onto the carbon cryogel electrodes in the membrane capacitive deionization mode. Moreover, the electrode can remove most of the adsorbed salt ions after full desorption with an excellent regeneration in the next adsorptions, indicating that the dual doping cryogel electrode is suitable for membrane capacitive deionization.

Keywords: Carbon cryogel; Thiourea; Dual doping; Membrane capacitive deionization

1. Introduction

Recently, the shortage of fresh water resource has become an increasingly serious problem due to extreme drought, population explosion, industrial consumption and water contamination. To solve this problem, researchers have shown great interest in proposing and developing desalination technologies, *e.g.*, distillation, reverse osmosis and electrodialysis [1–3]. However, limitation factors of these methods including high cost, high requirement for the device maintain and poor energy efficiency are quite evident and hinder the practical application [4]. Among the processes used for desalination, capacitive deionization (CDI) process is an energy-efficient and economical tech-

nology for desalination of low or medium salty water, and hence considered to be a promising deionization process in future [5,6].

The mechanism of the CDI process is simple to understand, where the salty water is passed through a spacer channel between electrodes with the opposite charges, and cations/anions from the salty water are adsorbed onto the porous space of the cathode and anode, respectively, yielding fresh water with low salinity. Subsequently, the absorbed ions can be released upon relaxation of the applied potential enabling the regeneration of the electrodes. The adsorption capacity primarily depends on the electrochemical adsorption and the physical adsorption. The electrical double layer (EDL) model and the pseudo capacitive model can be used to explain the theoretical adsorption process [5,7]. Based on these principles, the surface functional groups and porous

*Corresponding author.

structure of electrode material are crucial for a high-performance adsorption effect in the CDI process.

Various materials have been developed as electrode materials in the CDI cell, such as activated carbon [8], carbon cloth [9], carbon aerogel [10], carbon nanotubes [11], electro-spun carbon fiber [12], graphene aerogel [13], 3D graphene mesh [14], 3D mesoporous graphene sheet–sphere [15], rGO/Co₃O₄ [16], nickel-based intercalation compound [17], Bi foam [18] and metal–organic frameworks (Al-based [19], Zn-based [20] and Co-based [21]). In particular, carbon aerogels and cryogels, stacked by particles or sheets, show a medium specific surface area (400 ~ 1100 m²/g), high conductivity (25 ~ 100 S/cm) and low mass density (< 0.1 g/cm³), especially suitable for ions removal and water desalination [22]. On the other hand, the incorporation of heteroatoms within the carbon matrix can provide pseudo-capacitive effects and enhance wettability of carbon surface, which favors the electrode/electrolyte interactions and accelerates the diffusion of the salt ions towards the electrode surface [23]. The heteroatoms serving as donor or acceptor in the carbon electrode can adjust the potential of zero charge (E_{PZC}) and the oxidation state. E_{PZC} is a fundamental parameter of the electrode, defined as no net charge on the surface of the electrode, and anion-adsorption in CDI process occurs when the applied potential is higher than E_{PZC} , otherwise it is occurrence of cation-adsorption [24,25]. Nitrogen-doped carbon aerogels (cryogels) have been synthesized and applied in capacitive deionization [26–30]. To gain the synergistic effect of heteroatoms, dual heteroatoms doped carbon materials are also potential candidates attractive to be applied in CDI. However, the researches of dual doping carbon cryogel materials in CDI field are scarce.

In the CDI process, co-ions leave easily the electrodes upon reaching equilibrium during ion adsorption, and the repeated charge/discharge processes can result in oxide layer formation on the surface of the carbon material which causes changes in the E_{PZC} and hinders the salt removal efficiency [31,32]. To avoid the removal capacity fading, Pasta et al. demonstrated the novel hybrid capacitive deionization (HCDI) system, consisting of a capacitive electrode from CDI and a battery electrode, delivering superior deionization capacity [16,33]. Zhou et al. used Na₄Ti₉O₂₀ and activated carbon to assemble an asymmetrical capacitive deionization (A-CDI) technique for high salt removal capacity [34]. Gao et al. proposed the inverted capacitive deionization (i-CDI) system using modified carbon anode with –COO[–] group and cathode with –NH₃⁺ group, Biesheuvel et al. have fully discussed the dynamic model based on EDL model [35]. However, the narrow voltage window (≤ 1.1 V) should widen for its further development [36,37]. Particularly, the membrane capacitive deionization (MCDI) consisting of porous carbon material and ion exchange membrane (IEM) can sustain the desalination performance for long working time. This is due to the IEMs block co-ion expulsion and the increase in absorbed counter ions to neutralize these co-ions, leading to high salt removal efficiency and stable deionization performance [17,25,38,39]. At the same time, the macropores within the carbon materials and interface of IEMs provides extra storage space for the ions, contributing to the enhanced adsorption capacity in the MCDI process compared to that in the CDI process. To the best of our knowledge, there is no report on the co-doped carbon cryo-

gel materials in the MCDI application. Herein, the nitrogen and sulfur co-doped carbon cryogel (NSCC) were prepared by a sol-gel process using thiourea as the nitrogen/sulfur source. The influences of dual doping on the structural- and electrosorption properties were studied via scanning electron microscopy (SEM), X-ray photoelectron spectroscopy (XPS) and Fourier transform infrared spectroscopy (FT-IR). Moreover, the adsorption difference in NSCC electrodes in the CDI and the MCDI is also compared.

2. Experimental

2.1. Preparation of carbon cryogels

Thiourea (purity ≥99.5% wt.%) and resorcinol (purity ≥ 99.5% wt.%) were purchased from Tianjin Fuchen Chemical Co., Ltd. Formaldehyde (36 wt.% aqueous solution) was purchased from Shantou Xilong Chemical Co., Ltd. Ion exchange membranes (SELEMION™) were supplied by AGC Engineering Co., Ltd. All commercial chemicals were used without additional purification. Firstly, resorcinol, thiourea and Na₂CO₃ were mixed to form a homogeneous suspension solution, formaldehyde was thereafter added into the solution and stirred for 30 min. The reaction mechanism of thiourea with resorcinol and formaldehyde is depicted in Fig. 1. In this study, the molar ratio of thiourea/resorcinol (T/R ratio) was set to be 0:1, 0.1:1, 0.2:1 and 0.3:1, respectively. The solution was then transferred to ampoules with water bath at 85°C for 72 h. The organic cryogels were obtained after freeze-drying and identified as organic TRF-*x*, where *x* represents the T/R ratio. Afterwards, it was carbonized at 800°C for 2 h under N₂ atmosphere, the inorganic cryogels were denoted as NSCC-*x*. The carbon cryogels, acetylene black and polytetrafluoroethylene dissolved in N-Methyl-2-pyrrolidone in a weight ratio of 75:15:10 were mixed to obtain a rubber-like mud, and coated on the cycloid nickel foam (φ 1.5 cm) for capacity analysis. After drying at 80°C overnight, the electrodes were pressed densely under the pressure of 10 MPa. As for the electrochemical adsorption test, the thin mud electrode (~15 mg/cm²) weighed by an analytical balance (Mettler Toledo, d = 0.001 mg) was in a rectangle shape of 4 cm × 6 cm coated on the nickel foam (6 cm × 8 cm).

2.2. General characterization

Scanning electron microscopy (SEM; S-7800 Hitachi) was used to characterize the morphology of samples. X-ray single crystal diffraction (XRD, Bruker AXS D8 ADVANCE), Fourier transform infrared spectroscopy (FT-IR, PerkinElmer Spectrum RXI) and thermogravimetric analyzer (TG, Mettler Toledo DSC Thermal Analyzer) were used to determine the structural properties. X-ray photoelectron spectroscopy (XPS, Thermo ESCALAB 250) and elemental analyzer (Elementar Analysensysteme GmbH) were applied to analyze the detailed composition.

Galvanostatic charge/discharge experiments (GCD) were conducted using aBT-4Arbin battery tester. The specific capacitance (*C*, F/g) measured by galvanostatic test is calculated by the equation $C = (2I \Delta t) / (m \Delta U)$, where *I* (A), *m* (g), Δt (s) and ΔU (V) are the applied current, active mass,

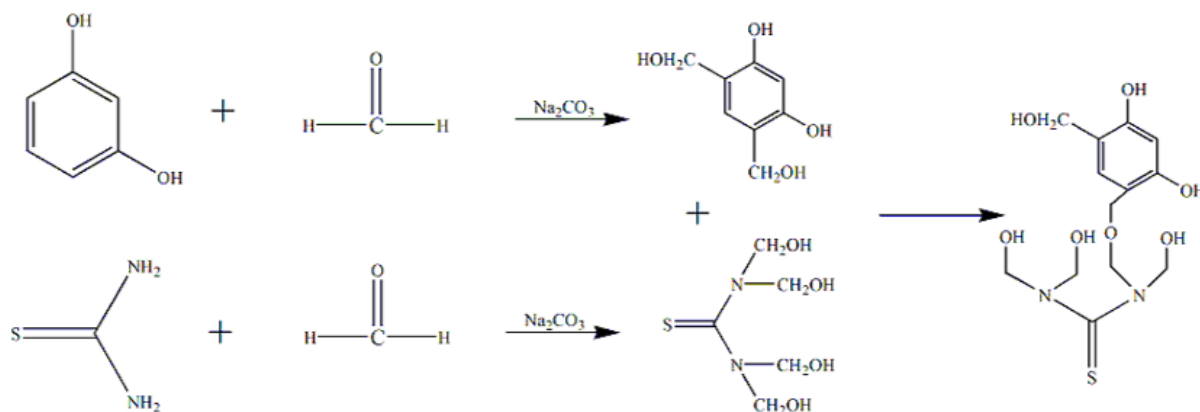


Fig. 1. Reaction of thiourea with resorcinol and formaldehyde during the sol-gel process.

discharging time and voltages difference, respectively. Cyclic voltammetry (CV) was performed using an electrochemical workstation (Zahner Enniun PP201, Germany) using a three-electrode system, where platinum foils and saturated calomel electrode were used as counter and reference electrodes, respectively. The specific capacitance was calculated by the enclosed area of the CV curves according to the following equation $C = (\int Idv)/(vm \Delta U)$, where C (F/g), I (A), v (mV/s), m , (g) and ΔU (V) are the specific capacitance, responding current, scanning rate, active mass and potential window, respectively.

2.3. Electrosorption test

Fig. 2 shows schematic diagrams of the CDI and MCDI system, which consist of anode/cathode electrodes with a polypropylene membrane [38]. These devices are compressed/bolted into the Polytetrafluoroethylene (PTFE) housing. The major difference between CDI and MCDI is that anion ion exchange membrane (AEM) and cation ion exchange membrane (CEM) are placed on the surface of anode (positive) electrode and cathode (negative) electrode, respectively. NaCl solution was controlled at a constant flow rate of 20 mL/min by a Longer BT100-2J wriggle pump until the conductivity of NaCl solution was below 3 $\mu\text{S}/\text{cm}$. A FeiloDDSJ-308A conductometer was used to track changes in the electrical conductivity of the salty water at the outlet. The adsorption capacity was calculated according to equation $q = (C_0 - C)V/m$, where q (mg/g), C_0 (mg/L), C (mg/L), V (L) and m (g) are the adsorption capacity, raw concentration, residual concentration of the solution, solution volume and active mass, respectively. The adsorption equations of Langmuir isothermal adsorption and Freundlich isothermal adsorption are listed in Eq. (1) and Eq. (2) to simulate the adsorption process.

$$q = \frac{q_m K_L C}{1 + K_L C} \quad (1)$$

$$q = K_F C^{1/n} \quad (2)$$

where C (mg/L), q (mg/g), q_m (mg/g), K_L and K_F are the equilibrium concentration of salt solution, adsorption

of equilibrium, achieved maximum adsorption capacity, Langmuir constant and Freundlich constant, respectively [40]. The charge efficiency in CDI and MDI adsorption was calculated according to Eq. (3).

$$\Lambda = \frac{(C_0 - C)VF}{\int Idt} \times 100\% \quad (3)$$

where Λ (%), C_0 (mg/L), C (mg/L), V (L), F (C/mol), I (A) and t (s) are the charge efficiency, initial concentration, residual concentration, total volume of salty solution, Faraday constant, responding current and adsorption time, respectively.

3. Results and discussion

3.1. Microstructural and morphological analysis of NSCCs

To confirm the interactive reaction between resorcinol, formaldehyde and thiourea, FT-IR spectra was used to characterize TRF-0 and TRF-0.2 before carbonization process. In Fig. 2a, the spectrum of TRF-0 precursor shows a broad O–H absorption peak at around 3400 cm^{-1} , and C=O stretching peaks at 1744 cm^{-1} and at 1378 cm^{-1} due to O–H stretching, indicating the presence of hydroxyl groups and carboxyl groups. In contrast, the organic TRF-0.2 precursor exhibits strong absorption peaks of C=C (1610 cm^{-1}) due to the π - π conjugated structure of benzene ring, C–N (1476 cm^{-1}) and C=S (784 cm^{-1}) due to grafted thiourea [41,42]. TG experiments were performed to determine the decomposition behavior under N_2 atmosphere from 30 to 900°C at the heating rate of $5^\circ\text{C}/\text{min}$. As shown in Fig. 3, the mass loss of the TRFs around 100°C is mainly due to the removal of oxygen-functional groups and attached micromolecules. With increasing T/R ratio, the mass loss of TRF samples becomes clearly visible at the same temperature, indicating a reduced thermal stability due to the addition of more thiourea. The residual mass of the TRFs is stabilized above 800°C , thus the temperature of 800°C is chosen for the pyrolysis of organic cryogel.

After pyrolysis, the elemental composition of NSCCs was characterized by organic elemental analysis (see Table 1). The doped contents of heteroatoms gradually increase with an increase in T/R ratio, and the highest content of heteroat-

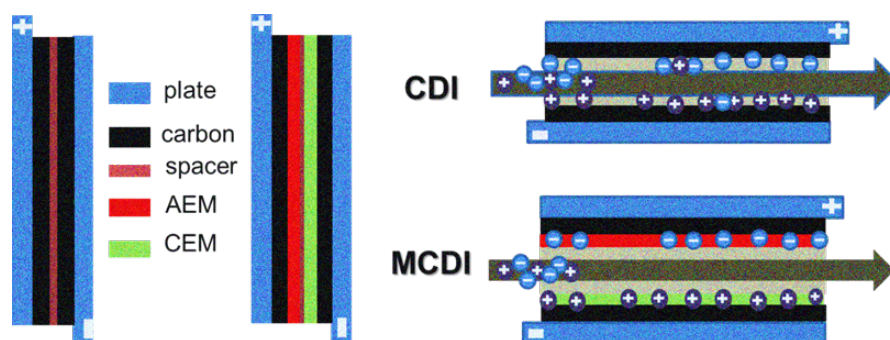


Fig. 2. Schematic diagram of the entire CDI and MCDI operating system.

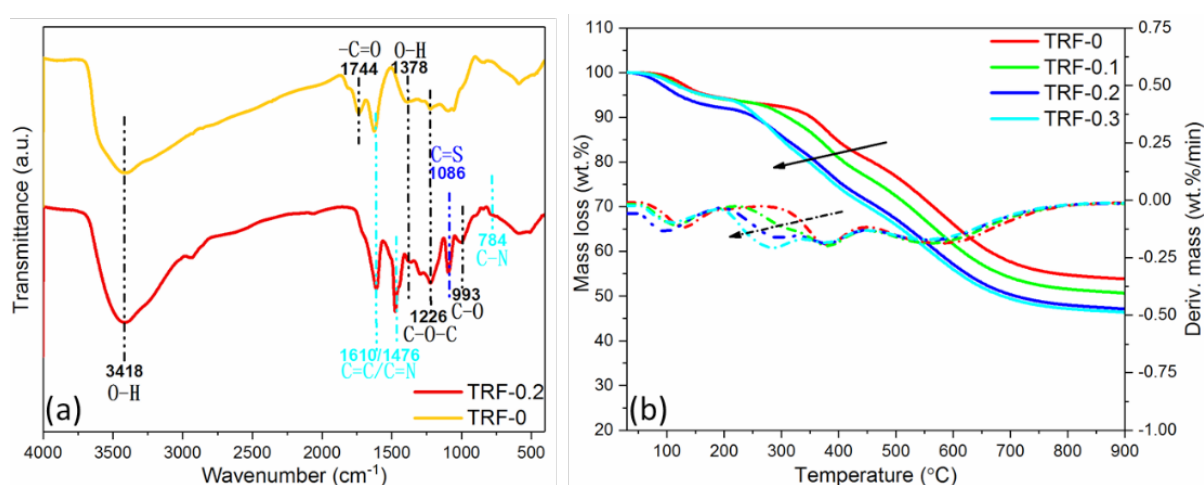


Fig. 3. (a) FT-IR spectra and (b) TG analysis of the TRF aerogels.

Table 1
Element composition of the NSCCs

Sample	Elemental content (wt.%)				
	C	O	N	S	(N+S)/C
NSCC-0	96.76	3.24	–	–	–
NSCC-0.1	95.14	3.46	0.91	0.49	1.47
NSCC-0.2	94.29	4.00	1.26	0.45	1.81
NSCC-0.3	93.75	4.08	1.69	0.48	2.31

oms is found in TRF-0.3, and the content of N and S species can reach as high as 1.69 wt.% and 0.48 wt.%, respectively. XPS analysis was performed to confirm the incorporation of heteroatoms in the NSCCs. Fig. 4a displays the XPS spectra, where the main elements are detected with peaks at about 162 eV (S2p), 285 eV (C 1s), 400 eV (N 1s) and 532 eV (O 1s), respectively. Particularly, the binding energies for the NSCC-0.2 obtained by fitting XPS spectra are listed in Figs. 4b–d. The peaks of C1s in Fig. 4b can be divided into 284.77 eV (C-C/C=C), 285.97 eV (C-O), 288.97 eV (C=O) and 288.97 eV (O-C=O), corresponding to atom content of 55.59%, 10.30%, 6.01% and 28.10%, respectively. The peaks of N 1s in Fig. 4c are split into three peaks at 398.87 eV, 400.87 eV and 401.97 eV, corresponding to pyrrole N (N-6), pyrrolic N (N-5) and

graphitic N (N-Q), respectively [43]. In Fig. 4d, the surface Scan can be deconvoluted into three peaks: S 2p_{2/3} (164.06 eV), S 2p_{1/2} (165.06 eV) and SO_x (168.86 eV) [44,45]. These results demonstrate that thiourea was successfully incorporated into the cryogel material through the polymerization reaction, and N and S elements have been doped in NSCCs via carbonization, which can modify the electron donor/acceptor properties and enhance Faradaic pseudocapacitance. This is because doping of N/S species can provide more active sites, improving the specific adsorption capacity and pseudocapacitance [46]. The doping behavior can also introduce defects and distortion in the carbon matrix, and the presence of heteroatoms can enhance charge density and wettability, facilitating the ion access to the surface and increasing charge accumulation [47–49].

As can be seen in Figs. 5a–d, particle sizes gradually increase with increasing T/R ratio, leading to an enhanced mechanical strength. This is because the volume shrinkage of the TRFs is suppressed after freeze drying. The N₂ adsorption-desorption curves of NSCCs in Fig. 6a are Type IV, where a hysteresis loop in the pressure range of P/P₀ = 0.4 ~ 0.9 is evidently observed, indicating the existence of mesoporous structure. The specific surface area slightly decreases from 620.5 m²/g (NSCC-0) to 555.7 m²/g (NSCC-0.3) and thereby decreases the average size from 17.9 (NSCC-0) to 17.7 nm (NSCC-0.3) (see Fig. 6b). The reason for this decrease is the decrease in the enlarged particle size of micropores and

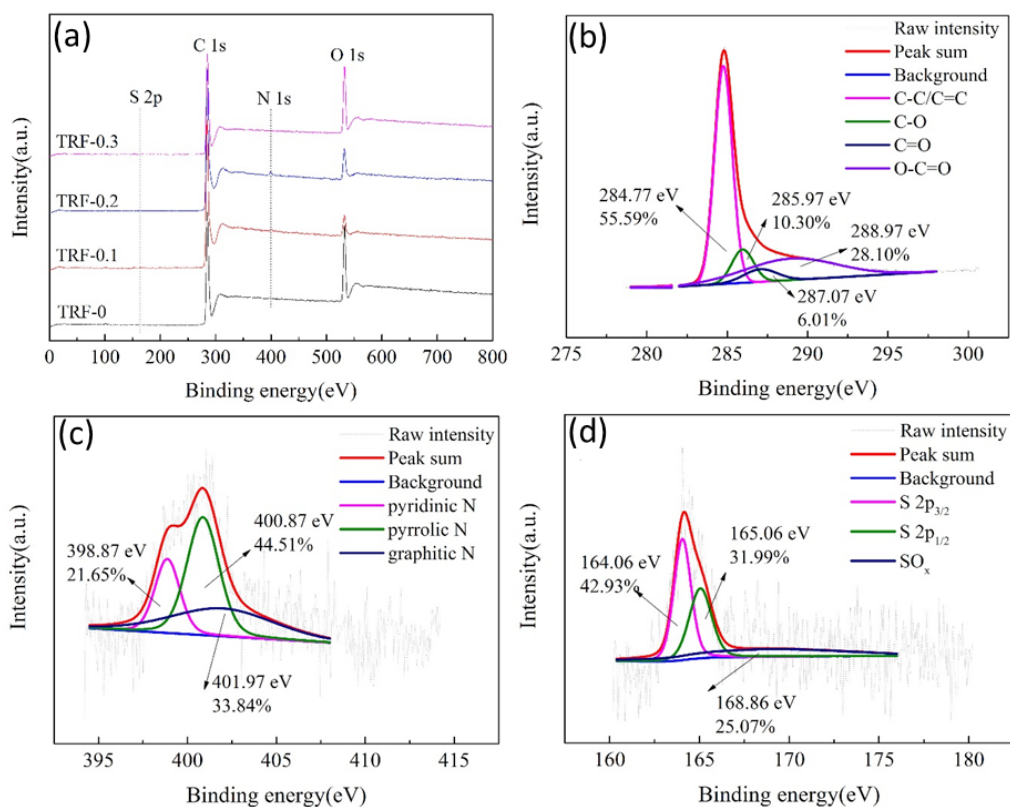


Fig. 4. XPS spectra: (a) XPS survey-scan spectra for NSCCs; (b) C 1s XPS spectra of NSCC-0.2; (c) N 1s XPS spectra of NSCC-0.2; (d) S 2p XPS spectra of NSCC-0.2.

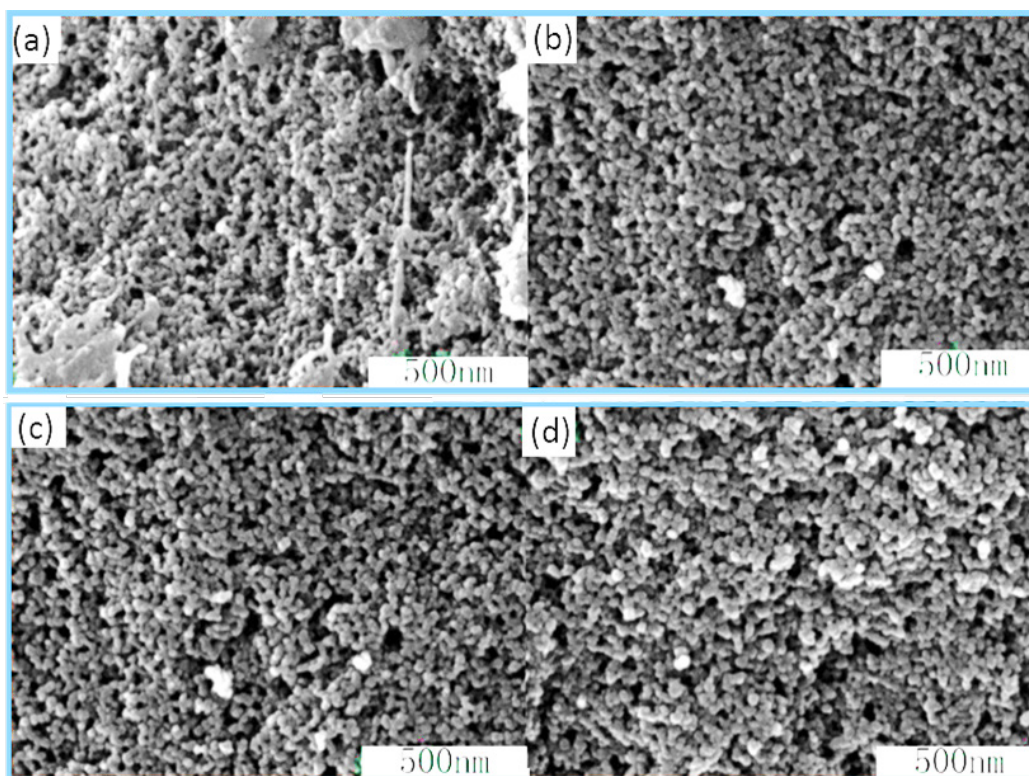


Fig. 5. SEM images: (a) NSCC-0; (b) NSCC-0.1; (c) NSCC-0.2; (d) NSCC-0.3.

hence increasing the mesopores. This can improve effective surface area and active pore volume, which is beneficial for ion storage in electrosorption [50,51]. Thus, the NSCCs are suitable electrode materials for electrosorption process.

3.2. Electrochemical properties of NSCCs

Fig. 7a displays typical galvanostatic curves of NSCCs measured by GCD method. As listed in Table 2, the longer charging/discharging time of NSCC-0.2 indicates its higher capacitance (182F/g) compared to NSCC-0 (166F/g). The deviations of the galvanostatic curves are resulting from the quick Faradic reactions at the heteroatomactive sites [52]. In Fig. 7b, the rate charging curves of NSCC-0.2 show symmetrical triangular shapes at different current densities, indicating an excellent cycle stability of the NSCC-0.2. Similarly, the CV curves show an approximately rectangular shape, which suggests that the layer-based ion adsorption plays a main role in the adsorption process, and it also displays stable cyclic characteristics [53]. Compared to NSCC-0, the NSCC-0.2 has the largest enclosed area (see Fig. 7c). The calculated specific capacitance derived from CV tests agree well with GCD results. In Fig. 7d, the rate-dependent CV curves over a scan range of 5–200 mV/s exhibit that the NSCC-0.2 change very slightly, even at the high scan rate of 200 mV/s, indicating a fast charge capability including double layer capacitance and pseudocapacitance.

3.3. Adsorption performance and kinetics of NSCCs

All electroadsorption experiments were performed at a constant temperature of 25°C, a constant circular flow of 20 mL/min and 200mL NaCl solution with an initial conductivity of 400 $\mu\text{S}/\text{cm}$ as brackish water. In Fig. 8a, the capacities of the NSCC-0 and NSCC-0.2 electrodes in the CDI are compared. It is very clear that the solution conductivity of the NSCC-0.2 decreases dramatically compared to that of the NSCC-0 at the same voltage. The electrosorption capacitances of NSCC-0.2 in Fig. 8b are higher than those of NSCC-0 at different voltages. The ion removal capacity of the NSCC-0.2 was generally higher than that of the NSCC-0, which is much palatable to previous electrochemical property. This

confirms that the NSCC-0.2 electrode is more suitable for the CDI process due to N and S co-doping. The electrosorption capacity of NSCC-0.2 electrode in the CDI and MCDI was also compared in Figs.9a and b. Conductivity curves for the MCDI process decrease sharply, and electrosorption capacitance slowly increases with increasing voltage in the CDI process, CDI mode had a lower adsorption capacity and longer adsorption time for equilibration than MCDI, the number of ions adsorbed to the electrode surface gradually decreased due to the electrosorption capacity limit. Due to IEMs placed in front of the electrodes in MCDI, the co-ions expelled from the micropores were blocked by the IEM and accumulated in the interparticle pore space, which increases the co-ion concentration within macropores, resulting in high electroadsorption values [54]. In the MCDI process, electrosorption capacitance proportionally increases with increasing voltage because of the selectively adsorbed counter-ions and repelled co-ions in IEMs. Saturation time required for MCDI (60 min) was longer than that for CDI (40 min).

In Figs. 10a–e, the conductivities of NSCC-0.2 in the CDI and the MCDI at different NaCl concentrations are depicted. IEMs have abundant charged groups such as sulfonic acid groups and quaternary amine groups, which can selectively adsorb counter-ions (ions of opposite polarity to the electrode) and repel co-ions (ions of equal polarity as the electrode) [38]. The CDI and MCDI tests at 0 V were used to compare pure physical adsorption, and no obvious difference of conductivity is observed. In general, the conductivity will reach the equilibrium status after 20 min, and it is the same for the CDI-1.2V. However, the MCDI-1.2V needs a longer time to reach equilibrium status, indicating a

Table 2
Specific capacity of the NSCCs

Sample	Specific capacity (F/g)			
	1 mA	2 mA	5 mA	10 mA
NSCC-0	166.06	151.60	132.78	121.39
NSCC-0.1	133.55	120.53	102.99	86.77
NSCC-0.2	182.95	168.83	153.58	132.57
NSCC-0.3	158.90	145.19	122.87	97.16

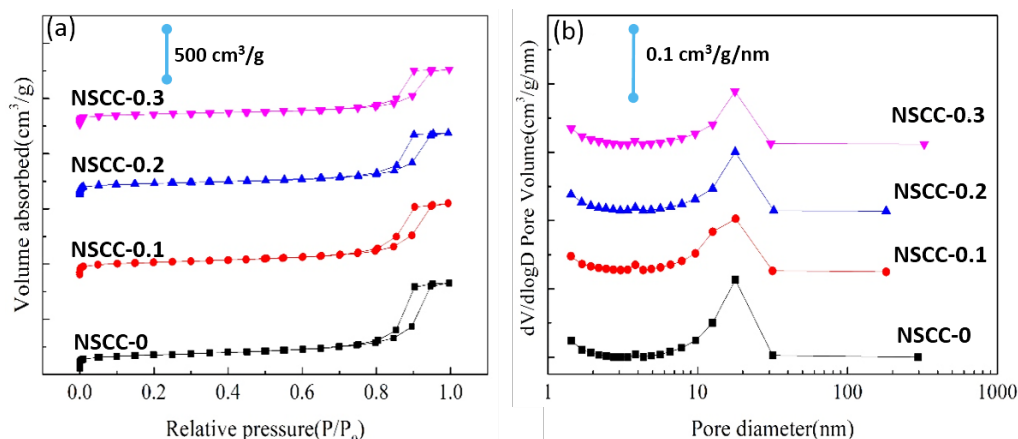


Fig. 6. N_2 adsorption isotherms and pore size distribution of NSCCs: (a) N_2 adsorption isotherms; (b) Pore size distribution.

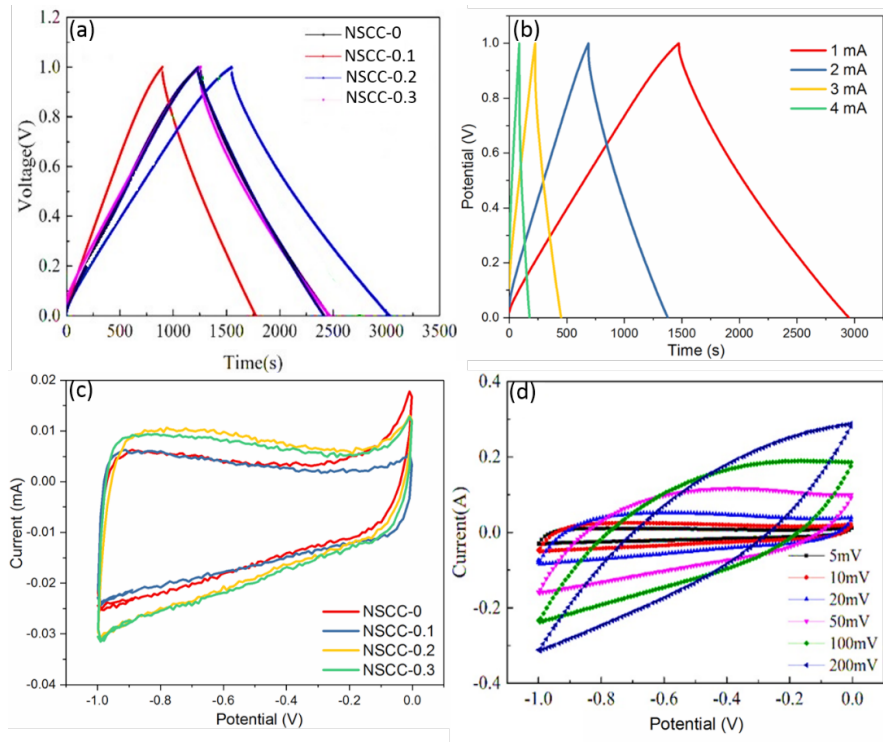


Fig. 7. (a) GCD curves of NSCCs at 1 mA; (b) GCD curves of NSCC-0.2 at different current; (c) CV curves of NSCCs at 5 mV/s; (b) CV curves of NSCC-0.2 at different scanning rates.

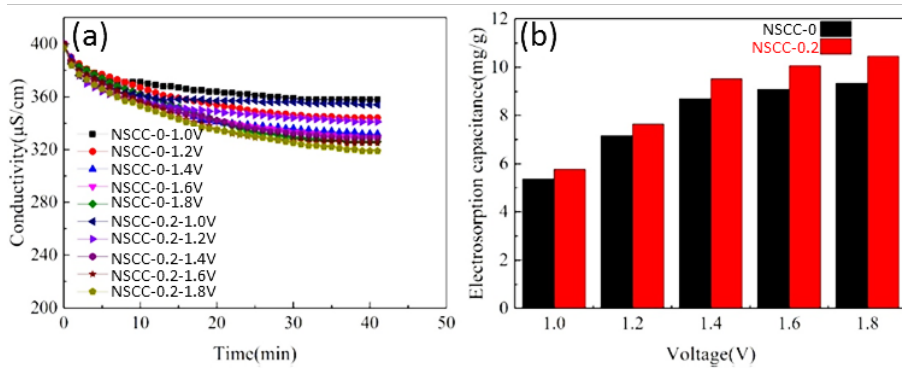


Fig. 8. The comparison of electroadsorption of NSCC-0 with NSCC-0.2 in CDI: (a) the conductivity of NaCl solution; (b) Adsorption capacity.

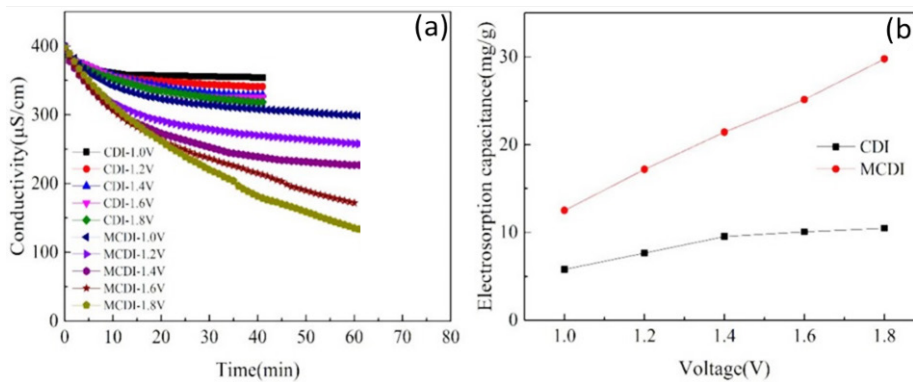


Fig. 9. The comparison of electroadsorption of NSCC-0.2 in CDI and MCDI: (a) the conductivity of NaCl solution; (b) Adsorption capacity.

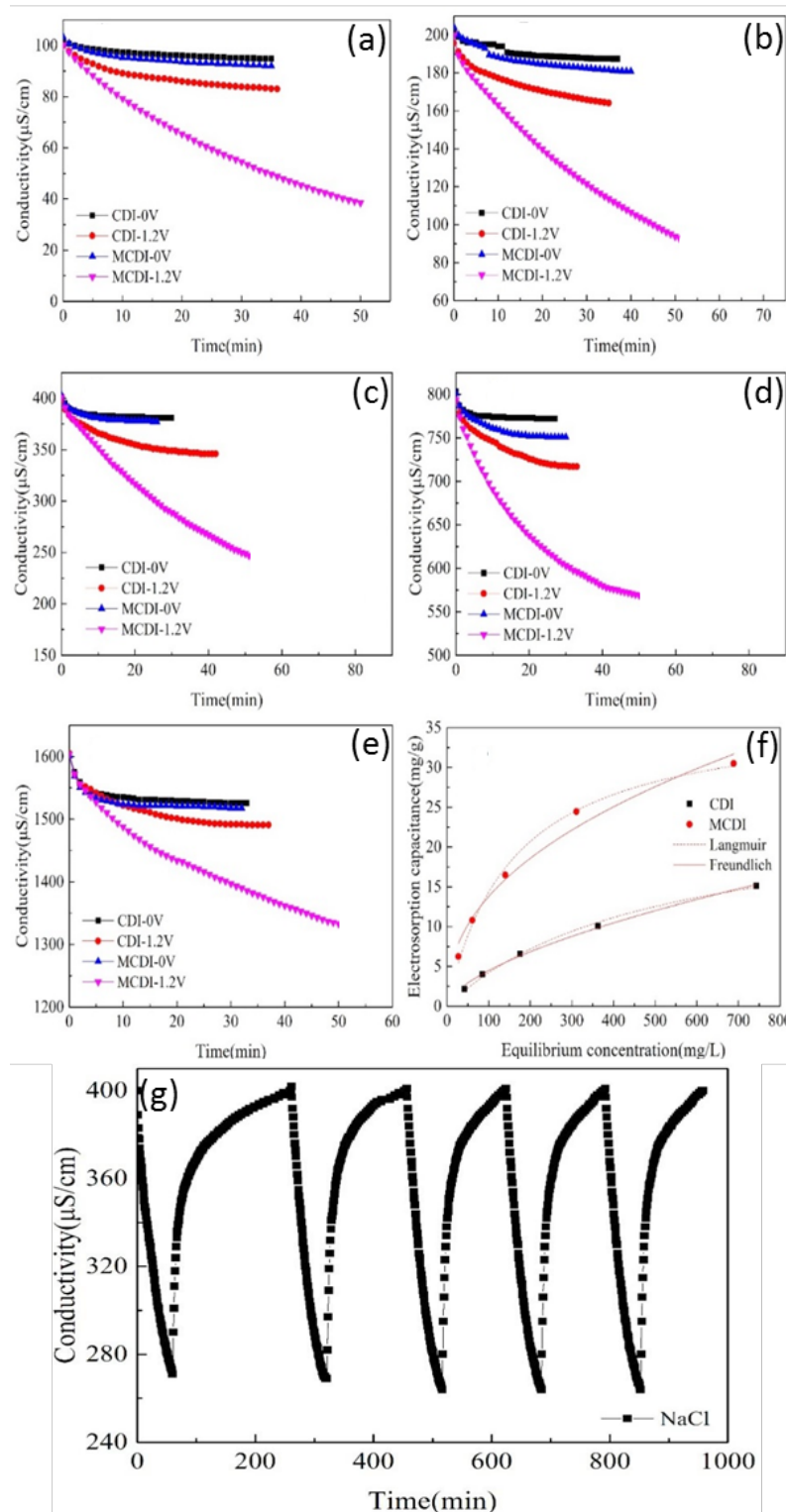


Fig. 10. Electrosorption of NSCC-0.2 in CDI and MCDI for different concentrations of NaCl solution: (a–e) the conductivity of NaCl Solution; (f) Electrodesorption isotherms; (g) cyclic adsorption-desorption experiments of NSCC-0.2 electrode in MCDI.

higher ion removal ability. As plotted in Fig. 10f, the adsorption results were simulated well by Langmuir and Freundlich isothermal adsorption, respectively. It is a complex dynamical process in which the chemical and geometrical

details of the electrode structure in MCDI, the cross-linked ion-exchange membranes as well as the details of the ion transportation flow in the stack cell system are crucial. The adsorption behavior of NaCl onto the composite elec-

Table 3

Comparison of charge efficiency in CDI and MCDI under different voltages

Voltage (V)	Λ_{CDI} (%)	Λ_{MCDI} (%)
1.0	67.89	92.14
1.2	59.86	88.98
1.4	40.18	80.08
1.6	39.56	70.79
1.8	31.14	65.80

trodes in MCDI was affirmed by the Freundlich isothermal model. The maximum adsorption capacity (37.16 mg/g) in the MCDI is significantly higher than that in the CDI (24.83 mg/g). The comparison of charge efficiency in the CDI and the MCDI as a function of voltages is listed in Table 3. The charge efficiency in the CDI gradually decreases to 31.14% with increasing working voltage to 1.8 V, but the charge efficiency in the MCDI still remains higher (65.8%). Fig. 10 g shows typical cyclic adsorption-desorption experiments of the NSCC-0.2 electrode in the MCDI. The NSCC-0.2 electrode can remove most of the adsorbed salt ions after desorption under 1.6 V, and adsorption capacity can still display an excellent regeneration in the next adsorption.

4. Conclusions

In conclusion, carbon cryogels containing sulfur and nitrogen heteroatoms were prepared and applied in the electroadsorption in this study. Thiourea is successfully incorporated into the cryogel material through the polymerization reaction, and N and S atoms have been doped in NSCCs via carbonization at 800°C. With increasing T/R ratio, particle sizes gradually increase, but the specific surface area and centered diameter distribution slightly decrease. It is found that NSCC-0.2 has a highest specific capacitance of 182.95 F/g and exhibits a stable cycling characteristic. The electroadsorption capacitance of NSCC-0.2 is higher than that of NSCC-0 at different voltages. In the MCDI, NSCC-0.2 has the higher adsorption capacity (37.16 mg/g) and higher charge efficiency (65.8%) at 1.8 V than those in the CDI (24.83 mg/g and 31.14%). The NSCC-0.2 electrode can remove most of the adsorbed salt ions after desorption with an excellent regeneration in the next adsorption. Thus, the NSCC-0.2 with a high capacity performance and a stable recyclability is more suitable for MCDI due to the mesoporous structure and sulfur-nitrogen doping improving adsorption properties.

Acknowledgment

It is a pleasure to acknowledge the generous financial support of this research by the National Natural Science Foundation of China (51372011) and China Scholarship Council (201506880029). The authors also appreciate the help from Geethu Balachandran and Zijian Zhao (Karlsruhe Institute of Technology), and Priyanka Sharma (Ludwig Maximilian University of Munich) for modification of this manuscript.

References

- [1] R.L. McGinnis, M. Elimelech, Global challenges in energy and water supply: the promise of engineered osmosis, *42*(23), (2008) 8625–8629.
- [2] C.J. Gabelich, T.D. Tran, I.H. Suffet, Electrosorption of inorganic salts from aqueous solution using carbon aerogels, *Environ. Sci. Technol.*, (2002) 3010–3019.
- [3] O.A. Hamed, Overview of hybrid desalination systems - Current status and future prospects, *Desalination*, 186 (2005) 207–214.
- [4] Q. Schiermeier, Water: Purification with a pinch of salt, *Nature*, 452 (2008) 260–261.
- [5] B. Jia, W. Zhang, Preparation and application of electrodes in capacitive deionization (CDI): a state-of-art review, *Nanoscale Res. Lett.*, 11 (2016) 64.
- [6] I. Cohen, E. Avraham, Y. Bouhadana, A. Soffer, D. Aurbach, The effect of the flow-regime, reversal of polarization, and oxygen on the long term stability in capacitive de-ionization processes, *Electrochim. Acta.*, 153 (2015) 106–114.
- [7] G. Tian, L. Liu, Q. Meng, B. Cao, Preparation and characterization of cross-linked quaternised polyvinyl alcohol membrane/activated carbon composite electrode for membrane capacitive deionization, *Desalination*, 354 (2014) 107–115.
- [8] T. Alencherry, N.A.R., S. Ghosh, J. Daniel, R. Venkataraghavan, Effect of increasing electrical conductivity and hydrophilicity on the electroadsorption capacity of activated carbon electrodes for capacitive deionization, *Desalination*, 415 (2017) 14–19.
- [9] C. Kim, P. Srimuk, J. Lee, S. Fleischmann, M. Aslan, V. Presser, Influence of pore structure and cell voltage of activated carbon cloth as a versatile electrode material for capacitive deionization, *Carbon*, 122 (2017) 329–335.
- [10] X. Quan, Z. Fu, L. Yuan, M. Zhong, R. Mi, X. Yang, Y. Yi, C. Wang, Capacitive deionization of NaCl solutions with ambient pressure dried carbon aerogel microsphere electrodes, *RSC Adv.*, 7 (2017) 35875–35882.
- [11] J. Lee, P. Srimuk, K. Aristizabal, C. Kim, S. Choudhury, Y.-C. Nah, F. Mücklich, V. Presser, Pseudocapacitive desalination of brackish water and seawater with vanadium-pentoxide-decorated multiwalled carbon nanotubes, *Chem. Sus. Chem.*, 10 (2017) 3611–3623.
- [12] Y. Belaustegui, S. Zorita, F. Fernández-Carretero, A. García-Luis, F. Pantò, S. Stelitano, P. Frontera, P. Antonucci, Electro-spun graphene-enriched carbon fibres with high nitrogen-contents for electrochemical water desalination, *Desalination*, 428 (2018) 40–49.
- [13] Z.Y. Leong, G. Lu, H.Y. Yang, Three-dimensional graphene oxide and polyvinyl alcohol composites as structured activated carbons for capacitive desalination, *Desalination*, (2017) in press.
- [14] J. Li, B. Ji, R. Jiang, P. Zhang, N. Chen, G. Zhang, L. Qu, Hierarchical hole-enhanced 3D graphene assembly for highly efficient capacitive deionization, *Carbon*, 129 (2018) 95–103.
- [15] Z.U. Khan, T. Yan, L. Shi, D. Zhang, Improved capacitive deionization by using 3D intercalated graphene sheet–sphere nanocomposite architectures, *Environ. Sci. Nano*, 5 (2018) 980–991.
- [16] G. Divyapriya, K.K. Vijayakumar, I. Nambi, Development of a novel graphene/Co₃O₄ composite for hybrid capacitive deionization system, *Desalination*, (2018) in press.
- [17] S. Porada, A. Shrivastava, P. Bukowska, P.M. Biesheuvel, K.C. Smith, Nickel hexacyanoferrate electrodes for continuous cation intercalation desalination of brackish water, *Electrochim. Acta.*, 255 (2017) 369–378.
- [18] D.H. Nam, K.S. Choi, Bismuth as a new chloride-storage electrode enabling the construction of a practical high capacity desalination battery, *J. Am. Chem. Soc.*, 139 (2017) 11055–11063.
- [19] Z. Wang, T. Yan, G. Chen, L. Shi, D. Zhang, High salt removal capacity of metal-organic gel derived porous carbon for capacitive deionization, *ACS Sustain. Chem. Eng.*, 5 (2017) 11637–11644.
- [20] Z. Wang, T. Yan, L. Shi, D. Zhang, In situ expanding pores of dodecahedron-like carbon frameworks derived from MOFs

- for enhanced capacitive deionization, *ACS Appl. Mater. Interfaces.*, 9 (2017) 15068–15078.
- [21] T. Gao, F. Zhou, W. Ma, H. Li, Metal-organic-framework derived carbon polyhedron and carbon nanotube hybrids as electrode for electrochemical supercapacitor and capacitive deionization, *Electrochim. Acta.*, 263 (2018) 85–93.
- [22] K.L. Yang, T.Y. Ying, S. Yiacoumi, C. Tsouris, E.S. Vittoratos, Electro sorption of ions from aqueous solutions by carbon aerogel: An electrical double-layer model, *Langmuir*, 17 (2001) 1961–1969.
- [23] D. Hulicova-Jurcakova, M. Seredych, G.Q. Lu, T.J. Bandoz, Combined effect of nitrogen- and oxygen-containing functional groups of microporous activated carbon on its electrochemical performance in supercapacitors, *Adv. Funct. Mater.*, 19(3) (2009) 438–447.
- [24] E. Pollak, I. Genish, G. Salitra, A. Soffer, L. Klein, D. Aurbach, The dependence of the electronic conductivity of carbon molecular sieve electrodes on their charging states, *J. Phys. Chem. B*, 110(14) (2006) 7443–7448.
- [25] A. Omosibi, X. Gao, J. Landon, K. Liu, Asymmetric electrode configuration for enhanced membrane capacitive deionization, *ACS Appl. Mater. Interfaces.*, 6 (2014) 12640–12649.
- [26] G. Tian, L. Liu, Q. Meng, B. Cao, Facile synthesis of laminated graphene for advanced supercapacitor electrode material via simultaneous reduction and N-doping, *J. Power Sources*, 274 (2015) 851–861.
- [27] G. Rasines, P. Lavela, C. Macías, M.C. Zafra, J.L. Tirado, J.B. Parra, C.O. Ania, N-doped monolithic carbon aerogel electrodes with optimized features for the electro sorption of ions, *Carbon*, 83 (2015) 262–274.
- [28] X. Xu, Z. Sun, D.H.C. Chua, L. Pan, Novel nitrogen doped graphene sponge with ultrahigh capacitive deionization performance, *Sci. Rep.*, 5 (2015) 1–9.
- [29] Y. Liu, T. Chen, T. Lu, Z. Sun, D.H.C. Chua, L. Pan, Nitrogen-doped porous carbon spheres for highly efficient capacitive deionization, *Electrochim. Acta*, 158 (2015) 403–409.
- [30] S. Zhao, T. Yan, H. Wang, G. Chen, L. Huang, J. Zhang, L. Shi, D. Zhang, High capacity and high rate capability of nitrogen-doped porous hollow carbon spheres for capacitive deionization, *Appl. Surf. Sci.*, 369 (2016) 460–469.
- [31] X. Gao, J. Landon, J.K. Neathery, K. Liu, Modification of carbon xerogel electrodes for more efficient asymmetric capacitive deionization, *J. Electrochem. Soc.*, 160 (2013) E106–E112.
- [32] E. Avraham, M. Noked, I. Cohen, A. Soffer, D. Aurbach, The dependence of the desalination performance in capacitive deionization processes on the electrodes PZC, *J. Electrochem. Soc.*, 158 (2011) 168–173.
- [33] H. Yoon, J. Lee, S. Kim, J. Yoon, Hybrid capacitive deionization with Ag coated carbon composite electrode, *Desalination*, 422 (2017) 42–48.
- [34] F. Zhou, T. Gao, M. Luo, H. Li, Heterostructured graphene@Na₄Ti₃O₂₀ nanotubes for asymmetrical capacitive deionization with ultrahigh desalination capacity, *Chem. Eng. J.*, 343 (2018) 8–15.
- [35] P.M. Biesheuvel, H.V.M. Hamelers, M.E. Suss, Theory of water desalination by porous electrodes with immobile chemical charge, *Colloid Interf. Sci. Commun.*, 9 (2015) 1–5.
- [36] X. Gao, A. Omosibi, J. Landon, K. Liu, Surface charge enhanced carbon electrodes for stable and efficient capacitive deionization using inverted adsorption–desorption behavior, *Energy Environ. Sci.*, 8 (2015) 897–909.
- [37] X. Gao, A. Omosibi, J. Landon, K. Liu, Enhanced salt removal in an inverted capacitive deionization cell using amine modified microporous carbon cathodes, *Environ. Sci. Technol.*, 49 (2015) 10920–10926.
- [38] S. Porada, R. Zhao, A. Van Der Wal, V. Presser, P.M. Biesheuvel, Review on the science and technology of water desalination by capacitive deionization, *Prog. Mater. Sci.*, 58 (2013) 1388–1442.
- [39] P.M. Biesheuvel, A. van der Wal, Membrane capacitive deionization, *J. Membr. Sci.*, 346 (2010) 256–262.
- [40] M. Mossad, L. Zou, Evaluation of the salt removal efficiency of capacitive deionisation: Kinetics, isotherms and thermodynamics, *Chem. Eng. J.*, 223 (2013) 704–713.
- [41] Q.F. Deng, L. Liu, X.Z. Lin, G. Du, Y. Liu, Z.Y. Yuan, Synthesis and CO₂ capture properties of mesoporous carbon nitride materials, *Chem. Eng. J.*, 203 (2012) 63–70.
- [42] G.-P. Hao, W.-C. Li, D. Qian, A.-H. Lu, Rapid synthesis of nitrogen-doped porous carbon monolith for CO₂ capture, *Adv. Mater.*, 22 (2010) 853–857.
- [43] C.N.R. Rao, K. Gopalakrishnan, A. Govindaraj, Synthesis, properties and applications of graphene doped with boron, nitrogen and other elements, *Nano Today*, 9 (2014) 324–343.
- [44] H.M. Jeong, J.W. Lee, W.H. Shin, Y.J. Choi, H.J. Shin, J.K. Kang, J.W. Choi, Nitrogen-doped graphene for high-performance ultracapacitors and the importance of nitrogen-doped sites at basal planes, *Nano Lett.*, 11 (2011) 2472–2477.
- [45] W. Gu, M. Sevilla, A. Magasinski, A.B. Fuertes, G. Yushin, Sulfur-containing activated carbons with greatly reduced content of bottle neck pores for double-layer capacitors: a case study for pseudocapacitance detection, *Energy Environ. Sci.*, 6 (2013) 2465.
- [46] Y. Wang, B. Zhang, M. Xu, X. He, Tunable ternary (P, S, N)-doped graphene as an efficient electrocatalyst for oxygen reduction reaction in an alkaline medium, *RSC Adv.*, 5 (2015) 86746–86753.
- [47] Y. Li, Y. Liu, M. Wang, X. Xu, T. Lu, C.Q. Sun, L. Pan, Phosphorus-doped 3D carbon nanofiber aerogels derived from bacterial-cellulose for highly-efficient capacitive deionization, *Carbon*, 130 (2018) 377–383.
- [48] L. Liu, X. Guo, R. Tallon, X. Huang, J. Chen, Highly porous N-doped graphene nanosheets for rapid removal of heavy metals from water by capacitive deionization, *Chem. Commun.*, 53 (2017) 881–884.
- [49] X. Gu, Y. Yang, Y. Hu, M. Hu, J. Huang, C. Wang, Nitrogen-doped graphene composites as efficient electrodes with enhanced capacitive deionization performance, *RSC Adv.* 4 (2014) 63189–63199. doi:10.1039/C4RA11468J.
- [50] J. Rouquerol, D. Avnir, C.W. Fairbridge, D.H. Everett, J.M. Haynes, N. Pernicone, J.D.F. Ramsay, K.S.W. Sing, K.K. Unger, Recommendations for the characterization of porous solids, *Pure Appl. Chem.*, 66(8) (1994) 1739–1758.
- [51] H. Bai, C. Li, G. Shi, Functional composite materials based on chemically converted graphene, *Adv. Mater.*, 23 (2011) 1089–1115.
- [52] C.T. Hsieh, H. Teng, Influence of oxygen treatment on electric double-layer capacitance of activated carbon fabrics, *Carbon*, 40 (2002) 667–674.
- [53] S.R.S. Prabaharan, R. Vimala, Z. Zainal, Nanostructured mesoporous carbon as electrodes for supercapacitors, *J. Power Sources*, 161 (2006) 730–736.
- [54] M. Noked, E. Avraham, A. Soffer, D. Aurbach, The rate-determining step of electroadsorption processes into nanoporous carbon electrodes related to water desalination, *J. Phys. Chem. C*, 113 (2009) 21319–21327.